2023 62nd IEEE Conference on Decision and Control (CDC)
December 13-15, 2023. Marina Bay Sands, Singapore

Safety of the Stanley Controller with Curved Lanes and Noisy Perception

Hongyi Li and Sayan Mitra

***Abstract*— The Stanley controller was designed for the DARPA 2005 Grand Challenge and has been widely used in real autonomous vehicles and simulation models. While the original paper presented an analysis of the tracking performance of this controller with straight roads, the analysis for general curved lanes and with perception errors is not available. We utilize Lyapunov theory to give tracking performance guarantees for the Stanley controller. Our analysis can be used for ensuring safety of lane following and provide guidelines for choosing design parameters with respect to velocity, lane curvation, and sensing constraints.**

I. INTRODUCTION

The Stanley controller was originally designed and implemented by the Stanford Racing Team, on a Volkswagen Touareg [1] as a part of the 2005 DARPA Grand Challenge. As a trajectory tracking controller for autonomous vehicles, it led the Stanford team to gain excellent performance in the competition and ultimately win in the Grand Challenge [2]. Since then, the Stanley controller has been used in many real systems, simulation models, and research prototypes. For instance, Amer *et al.* [3] combined a modified Stanley controller with particle swarm optimization to design path tracking controllers for autonomous armoured vehicles. Wang *et al.* [4] utilized genetic algorithms to optimize the Stanley controller for autonomous agricultural tractors. On the theoretical side, AbdElmoniem *et al.* [5] used the Stanley model for a predictive lateral controller. Hsieh *et al.* [6] used approximate abstractions to carry out a safety analysis when the state estimates came from computer vision models.

Although the Stanley controller and its variants have been used widely, to the best of our knowledge, a formal analysis of its tracking performance with respect to general curved roads has not been published. Further, the impact of sensing or perception error on this control strategy, an important consideration in any real system, has also not been analyzed. Understanding the tracking performance in detail can be the basis for safety analysis (verification) as well as synthesis of higher-level planners. The latter synthesis approach has been explored and implemented in a number of tools for different types of vehicles and controllers [7], [8].

In this paper, we provide a detailed Lyapunov-based analysis of the tracking performance of the Stanley controller, for a vehicle with the bicycle dynamics [9], following curved lanes, and using noisy sensors. With respect to the reference path, the key state variables of the vehicle's are the *crosstrack error* d and the *heading error* ψ. We will precisely define these quantities in Section II-A (see Figure 1). Let d_s and ψ_s represent the *sensed* crosstrack and heading errors. Let us assume the difference between the actual and the sensed values (sensing error) is at most e_d and e_ψ, respectively. The Stanley controller uses these sensed values (d_s, ψ_s) to compute the control signal, which is the steering angle δ. We visualize the key state variables—the actual crosstrack and heading errors (d, ψ)—under the action of the steering control as a point moving on the 2D plane. We take the point $(d, \psi) = (0, 0)$ as the equilibrium point and the system is unsafe when explicit finite upper bounds can't be guaranteed for the crosstrack and heading errors.

There are several challenges in this analysis. First, as the vehicle is following an arbitrary curved path, we have to perform a coordinate transformation to represent the crosstrack (d) and the heading (ψ) errors along a coordinate system that moves along the path. Second, the tracking performance analysis for a straight lane can be done using a standard Lyapunov function [6], but this function now has to be modified to accommodate path curvatures and sensing noise. Most importantly, because of the curvature, saturation in control, and the perception errors, we cannot expect the tracking errors to converge to zero from all possible initial conditions. Therefore, we have to carefully identify what region of the state space can guarantee explicit finite upper bounds for d and ψ. This region can be seen as an important outcome of the analysis, which gives the, so called, safe *operating design domain (ODD)*. The safe ODD for this problem turns out to be a symmetrical region around the equilibrium point in the state space, and the theoretical guarantee aligns with the extreme cases, where the path is maximally curving away from the vehicle and the sensing noise reaches the highest level. Our analysis shows a lower speed is safer when the car is very far away from the reference path. The analysis also implies the optimal controller gain increases inversely with the vehicle speed and shorter vehicles are easier to safely control. With these results, system designers can be more informed about choosing design parameters with respect to different vehicle speeds, lane curvatures and sensing constraints, and thus become confident when they use the Stanley controller.

In Section II, we first introduce the basic dynamics model for a vehicle following curved paths with noisy perception. With these sets of necessary knowledge, we continue to apply Lyapunov theory and analyze the results by numerical approximations in Section III. In Section IV, we further analyze how the vehicle speed, controller gain and vehicle length can

H. Li is a graduate student of Electrical and Computer Engineering at University of Illinois Urbana-Champaign, hli106@illinois.edu
S. Mitra is with Faculty of Electrical and Computer Engineering at University of Illinois Urbana-Champaign, mitras@illinois.edu

affect the area of safe ODD. Section V presents simulations, which further validate the safety of Stanley under curved paths and noisy perception. Section VI summarizes this paper, while Appendix contains detailed proofs that support the establishment of safe ODD around the equilibrium point in the state space.

II. General Stanley Controller

Section II-A introduces the vehicle model following a path and the sensing errors. Section II-B is about the dynamics of the Stanley controller, under the impact of sensing noise. Section II-C defines the path curvature and integrates it into the dynamics model.

A. Vehicle Model, Paths, and Sensing Errors

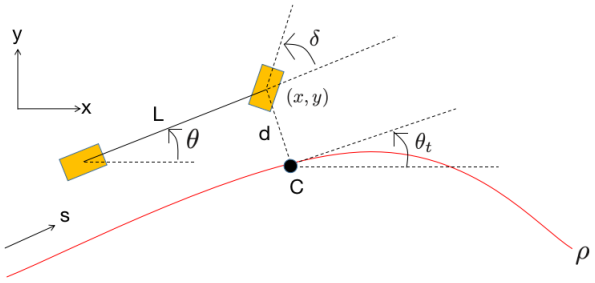

Fig. 1. Bicycle model, with the front wheels as guiding wheels. The left and right rectangular blocks represent the rear and front pairs of wheels, respectively. ρ is a continuously differentiable curve.

We will use the popular bicycle model [12] for the ground vehicle as depicted in Figure 1. Throughout this paper, (x, y) is the coordinate of the front wheel center and is considered as the position of the vehicle. Let L be the length of the car. The direction of the line joining the mid-points of the wheels is the vehicle's heading. The *heading angle* θ is the angle between the vehicle's heading and the x-axis in the world frame. The front wheels are used as guiding wheels: δ is the *steering angle*, which is the angle of the front wheel with respect to the vehicle's heading. The steering angle δ is the main control input of the vehicle.

The curve ρ represents the reference path the car is trying to follow. Let's denote the closest point to the vehicle position (x, y) on the reference path as the *critical point* (point **C** in Figure 1). θ_t represents the angle between the path's tangent at **C** and the x-axis in the world frame. The *crosstrack error*, d, represents the distance between (x, y) and point **C**. In fact, d is positive when the vehicle is on the left side of the reference path and vice versa.

In Figure 1, $s \in \mathbb{R}_{\geq 0}$ represents the distance that the car has travelled along the reference path. Conceptually, this distance is equal to the total curve length on the reference path between the current and initial critical points. For example, in Figure 2, while the car is moving from **P1** to **P2**, the critical point moves from **C1** to **C2** on the reference path. In this case, the distance s is one fourth of the circle circumference.

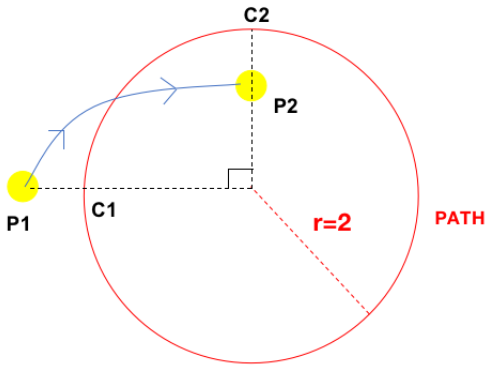

Fig. 2. Distance that the vehicle travels along a circle. The balls represent the car's positions. The circle represents the reference path. The arrows represent the car's trajectory.

Aside from the crosstrack error d, we define the *heading error* ψ as:

$$\psi = \theta - \theta_t, \tag{1}$$

which is the difference between the car's heading (θ) and the reference path's heading (θ_t) at the current critical point. For the calculations of both crosstrack and heading errors, the critical point needs to be estimated from sensors. For example, in a vision-based lane tracking system, as in [13], camera images are used to detect the lanes ahead of the vehicle and then the crosstrack and heading errors relative to the center of the lane are computed. Inevitably, this estimation introduces errors. In general, the estimation error characteristics can be quite complicated and state-dependent [6]. However, for now, we assume the following worst-case estimation error model:

$$d_s = d + e_d, \quad \psi_s = \psi + e_\psi, \tag{2}$$

where d_s is the sensed crosstrack error and $e_d \in [-\epsilon_d, \epsilon_d]$ is the bounded error in sensing d_s. Similarly, ψ_s is the sensed heading error and $e_\psi \in [-\epsilon_\psi, \epsilon_\psi]$ is the bounded error in sensing ψ_s. We are interested in understanding the performance of the Stanley controller with respect to the curvature of the lanes as well as the sensing error parameters, namely ϵ_d and ϵ_ψ.

B. Stanley Controller Dynamics

Disturbed by perception noise, the vehicle uses d_s and ψ_s to generate the steering angle δ in the Stanley model [1], as below.

$$\delta = \begin{cases} -\psi_s - arctan(\frac{K \cdot d_s}{v_f}) & |\psi_s + arctan(\frac{K \cdot d_s}{v_f})| < \delta_{max} \\ -\delta_{max} & \psi_s + arctan(\frac{K \cdot d_s}{v_f}) \geq \delta_{max} \\ \delta_{max} & \psi_s + arctan(\frac{K \cdot d_s}{v_f}) \leq -\delta_{max} \end{cases} \tag{3}$$

In (3), K denotes the positive controller gain, v_f represents the constant forward speed, and δ_{max} is the vehicle's maximum steering angle ($0 < \delta_{max} < \frac{\pi}{2}$). The first line in (3) is defined as *nominal region control*, while the last two lines are *saturated region control* [1]. Our analysis mainly

focuses on the nominal region, as the maximum steering angle is used to return from the saturated regions to the nominal region [1]. For the convenience of later calculations, we designate $\alpha(x) = arctan(\frac{K \cdot x}{v_f})$.

The kinematics for the crosstrack error is $\dot{d} = v_f \sin(\psi + \delta)$ [10]. Combining this with (3) and (2), we get:

$$\dot{d} = v_f \sin(\psi - \psi_s - \alpha(d_s)) = -v_f \sin(e_\psi + \alpha(d_s)). \quad (4)$$

We can then use the chain rule and (4) to calculate $\dot{\alpha}(d)$, which will be used in the Lyapunov analysis.

$$\begin{aligned}\dot{\alpha}(d) &= \frac{d}{dt} arctan\Big(\frac{K \cdot d}{v_f}\Big) = \frac{1}{1 + \frac{K^2 d^2}{v_f^2}} \frac{K}{v_f} \dot{d} \\ &= \frac{-K v_f^2}{v_f^2 + K^2 d^2} sin(e_\psi + \alpha(d_s)).\end{aligned} \quad (5)$$

C. Path Curvature at Critical Points

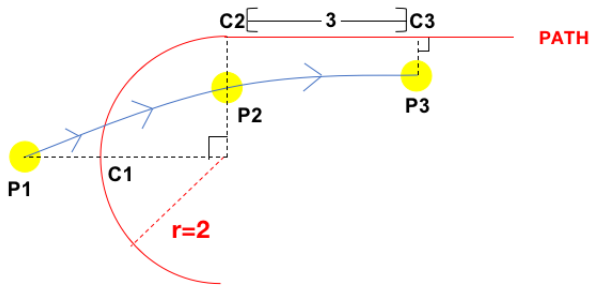

Fig. 3. Illustration of the reference path's curvature profile. The reference path consists of a curve (part of a radius-2 circle) and a straight line.

Each reference path has a curvature profile $c(\cdot) : \mathbb{R}_{\geq 0} \to \mathbb{R}$, which is a function of s (the distance that the vehicle has travelled along the reference path). Mathematically, the definition of curvature is $c(s) = \frac{d\theta_t}{ds}$. Let's suppose the vehicle and its corresponding critical point move along the reference path within an infinitesimal time period dt. The definition of curvature can then imply:

$$c(s) \cdot \frac{ds}{dt} = \frac{d\theta_t}{dt} \Longrightarrow c(s)\dot{s} = \dot{\theta}_t. \quad (6)$$

For example, in Figure 3, the initial position of the car ($s = 0$) is **P1** with **C1** as the critical point, which means $c(s) = \frac{1}{r} = \frac{1}{2}$ at **P1**. When the car moves from **P1** to **P2**, the critical point gradually moves from **C1** to **C2** on the reference path. As discussed previously, $s = \pi$ and thus $c(s) = \frac{1}{2}$ at **P2**. When the car later moves from **P2** to **P3**, the critical point gradually moves from **C2** to **C3** on the reference path, which means $s = \pi + 3$ and $c(s) = 0$ at **P3**.

The geometrical analysis in [10] also establishes:

$$\dot{s} = v_f cos(\psi + \delta) + \dot{\theta}_t d = v_f cos(e_\psi + \alpha(d_s)) + \dot{\theta}_t d. \quad (7)$$

By combining (6) and (7), we can get:

$$\dot{s} = \frac{v_f cos(e_\psi + \alpha(d_s))}{1 - d \cdot c(s)}, \dot{\theta}_t = \frac{v_f cos(e_\psi + \alpha(d_s)) c(s)}{1 - d \cdot c(s)}. \quad (8)$$

According to the derivation in [11], $\dot{\theta} = \frac{v_f tan(\delta)}{L}$. By combining this result with (1) and (8), we have:

$$\begin{aligned}\dot{\psi} &= \dot{\theta} - \dot{\theta}_t \\ &= -\Big(\frac{tan(\psi_s + \alpha(d_s))}{L} + \frac{cos(e_\psi + \alpha(d_s)) c(s)}{1 - d \cdot c(s)}\Big) v_f.\end{aligned} \quad (9)$$

III. Tracking Error Analysis

Throughout the analysis, we will make the following assumption, which states that the worst-case noise won't exceed the maximum steering input. This rules out uninteresting extreme values. Otherwise, any vehicle states in the nominal region will look like saturated states.

Assumption 1. $\epsilon_\psi + \alpha(\epsilon_d) < \delta_{max}$.

Next we will define a function based on tracking errors, and show that it satisfies the Lyapunov conditions inside the safe *operating design domain (ODD)*. In Section III-B, we will use this result to derive the upper bounds of tracking errors. A qualitative analysis is also done for the state space outside safe ODD. Section III-C puts these derived upper bounds and analysis results together, to show that (d, ψ) always stays within a certain distance from the equilibrium point.

A. Lyapunov Analysis

We define the Lyapunov function as a function of the crosstrack error d and the heading error ψ: $V(d, \psi) = |\psi + \arctan(\frac{K \cdot d}{v_f})| = |\psi + \alpha(d)|$. We choose this Lyapunov function because the sum $\psi + \alpha(d)$ can reflect the counter-effects when d and ψ are of opposite signs and equals to zero at the equilibrium point. For the convenience of calculations, we analyze the time derivative of $\big(V(d, \psi)\big)^2$. By applying the chain rule and combining (5) and (9), we can get:

$$\begin{aligned}&\frac{dV^2}{dt} = 2\big(\psi + \alpha(d)\big)\big(\dot{\psi} + \dot{\alpha}(d)\big) \\ &= -2v_f\big(\psi + \alpha(d)\big)\Big(\frac{tan\big(\psi_s + \alpha(d_s)\big)}{L} + \frac{cos\big(e_\psi + \alpha(d_s)\big) c(s)}{1 - d \cdot c(s)} \\ &+ \frac{K v_f}{v_f^2 + K^2 d^2} sin\big(e_\psi + \alpha(d_s)\big)\Big).\end{aligned} \quad (10)$$

We can partition the error space inside the nominal region as in Figure 4 and define the following four sub-regions.

- E_1: $d > 0$ and $A(d) < \psi < -\alpha(d)$
- E_2: Rotate E_1 by 180 degrees around the equilibrium point
- E_3: $d > 0$ and $-\alpha(d) < \psi < B(d)$
- E_4: Rotate E_3 by 180 degrees around the equilibrium point,

where $A(d)$ and $B(d)$ are defined as:

$$\begin{aligned}A(d) &= -arctan\Big(L\Big(\frac{sin(\epsilon_\psi)}{d} + \frac{K v_f}{v_f^2 + K^2 d^2}\Big)\Big) - \epsilon_\psi - \alpha(d + \epsilon_d) \\ B(d) &= arctan\Big(L\Big(\frac{1}{d} + \frac{K v_f \cdot sin(\delta_{max})}{v_f^2 + K^2 d^2}\Big)\Big) + \epsilon_\psi - \alpha(d - \epsilon_d).\end{aligned} \quad (11)$$

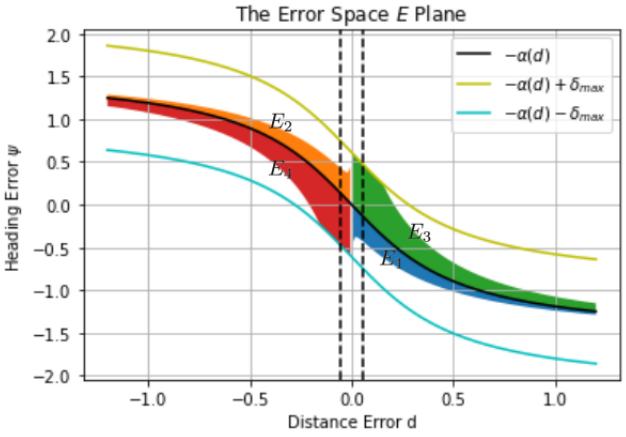

Fig. 4. Error space inside the nominal region. The two black dashed lines represent $d = \epsilon_d + \frac{v_f \cdot \tan(\epsilon_\psi)}{K}$ and $d = -(\epsilon_d + \frac{v_f \cdot \tan(\epsilon_\psi)}{K})$.

We define $E - (E_1 \cup E_2 \cup E_3 \cup E_4)$ as the safe *operating design domain (ODD)* and prove that the Lyapunov condition is guaranteed to hold in this region, even under arbitrarily large path curvatures and the most adversarial sensing noise. For the sake of convenience, let's denote $UE = E_1 \cup E_2 \cup E_3 \cup E_4$ and $SE = E - UE$. It's trivial to see $V(d, \psi) > 0$ for $(d, \psi) \in SE$.

Lemma 1. $\frac{dV^2}{dt} < 0$ *in* SE.

Proof: Suppose (d, ψ) is in the state space region below E_1 $\big(d > 0$ and $-\alpha(d) - \delta_{max} < \psi < A(d)\big)$. From the definition of E_1, we have:

$$\begin{aligned}\psi_s + \alpha(d_s) &\leq \psi + \epsilon_\psi + \alpha(d + \epsilon_d) \\ &< -arctan\Big(L\Big(\frac{sin(\epsilon_\psi)}{d} + \frac{Kv_f}{v_f^2 + K^2d^2}\Big)\Big),\end{aligned}$$

$$\frac{tan(\psi_s + \alpha(d_s))}{L} < -\frac{sin(\epsilon_\psi)}{d} - \frac{Kv_f}{v_f^2 + K^2d^2},$$

$$\frac{tan(\psi_s + \alpha(d_s))}{L} + \frac{sin(\epsilon_\psi)}{d} + \frac{Kv_f}{v_f^2 + K^2d^2} < 0. \quad (12)$$

From Theorem 1 in Appendix, we get $\frac{cos(e_\psi + \alpha(d_s))c(s)}{1 - d \cdot c(s)} < \frac{sin(\epsilon_\psi)}{d}$. $\frac{Kv_f}{v_f^2 + K^2d^2} sin(e_\psi + \alpha(d_s)) \leq \frac{Kv_f}{v_f^2 + K^2d^2}$ is also a trivial fact. By putting these two facts into (12), we get:

$$\begin{aligned}&\frac{tan(\psi_s + \alpha(d_s))}{L} + \frac{cos(e_\psi + \alpha(d_s))c(s)}{1 - d \cdot c(s)} \\ &\quad + \frac{Kv_f}{v_f^2 + K^2d^2} sin(e_\psi + \alpha(d_s)) < \quad (13) \\ &\frac{tan(\psi_s + \alpha(d_s))}{L} + \frac{sin(\epsilon_\psi)}{d} + \frac{Kv_f}{v_f^2 + K^2d^2} < 0.\end{aligned}$$

For the state space below E_1, $\psi + \alpha(d) < 0$. Plugging this and (13) into (10), we can get $\frac{dV^2}{dt} < 0$ for this region. The proof for the state space above E_2 is similar, due to symmetry.

Suppose (d, ψ) is in the state space above E_3 $\big(d > 0$ and $B(d) < \psi < -\alpha(d) + \delta_{max}\big)$. From the definition of E_3, we have:

$$\begin{aligned}\psi_s + \alpha(d_s) &\geq \psi - \epsilon_\psi + \alpha(d - \epsilon_d) \\ &> arctan\Big(L\Big(\frac{1}{d} + \frac{Kv_f \cdot sin(\delta_{max})}{v_f^2 + K^2d^2}\Big)\Big),\end{aligned}$$

$$\frac{tan(\psi_s + \alpha(d_s))}{L} > \frac{1}{d} + \frac{Kv_f \cdot sin(\delta_{max})}{v_f^2 + K^2d^2},$$

$$\frac{tan(\psi_s + \alpha(d_s))}{L} - \frac{1}{d} - \frac{Kv_f \cdot sin(\delta_{max})}{v_f^2 + K^2d^2} > 0. \quad (14)$$

By doing an analysis similar to Theorem 1 in Appendix, we get $\frac{cos(e_\psi + \alpha(d_s))c(s)}{1 - d \cdot c(s)} > -\frac{1}{d}$ and $\frac{Kv_f}{v_f^2 + K^2d^2} sin(e_\psi + \alpha(d_s)) > -\frac{Kv_f \cdot sin(\delta_{max})}{v_f^2 + K^2d^2}$. By putting these two facts into (14), we get:

$$\begin{aligned}&\frac{tan(\psi_s + \alpha(d_s))}{L} + \frac{cos(e_\psi + \alpha(d_s))c(s)}{1 - d \cdot c(s)} \\ &\quad + \frac{Kv_f}{v_f^2 + K^2d^2} sin(e_\psi + \alpha(d_s)) > \quad (15) \\ &\frac{tan(\psi_s + \alpha(d_s))}{L} - \frac{1}{d} - \frac{Kv_f \cdot sin(\delta_{max})}{v_f^2 + K^2d^2} > 0.\end{aligned}$$

For the state space above E_3, $\psi + \alpha(d) > 0$. Plugging this and (15) into (10), we can get $\frac{dV^2}{dt} < 0$ for this region. The proof for the state space below E_4 is similar, due to symmetry.

In this way, $\frac{dV^2}{dt} < 0$ in SE is proved. □

B. Tracking Error Bounds

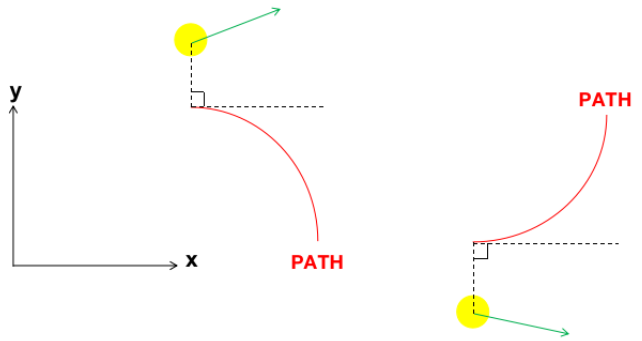

Fig. 5. Left: $d > 0$, $\psi > 0$. Right: $d < 0$, $\psi < 0$. (The arrows represent the car's heading directions.)

Based on the Lyapunov analysis, we can proceed to derive the following three statements, for bounds of tracking errors in three parts of the nominal region. Lemma 2 and 3 deal with the two parts that constitute safe ODD. Specifically, Lemma 2 deals with the cases, in which the car's heading doesn't comply with the reference path's direction while the path is curving away from the vehicle (Figure 5). Lemma 3 deals with the cases, in which the car's heading generally complies with the reference path's direction while the car isn't too close to the path (black dash lines in Figure 4). These two lemmas obtain explicit upper bounds for tracking

errors. Lemma 4 carries out a qualitative analysis to the state space outside safe ODD and proves a finite upper bound for $|d|$ exists.

Lemma 2. *When (d, ψ) stays in SE, and d is of the same sign as ψ, $|d|$ and $|\psi|$ have a finite upper bound.*

Proof: Let's denote the initial state as $d(t_0) = d_0$, $\psi(t_0) = \psi_0$ and thus $V(d_0, \psi_0) = \eta_0$. According to Lemma 1, $V(d(t), \psi(t)) \leq \eta_0$ for $t \geq t_0$. Now that $d(t)$ and $\psi(t)$ are of the same sign, $V(d(t), \psi(t)) = |\psi(t)| + |\alpha(d(t))|$. Hence, $|\alpha(d(t))| \leq V(d(t), \psi(t)) \leq \eta_0$ and $|\psi(t)| \leq V(d(t), \psi(t)) \leq \eta_0$, which means both of the crosstrack and heading errors are bounded. □

Lemma 3. *When (d, ψ) stays in SE, d is of the opposite sign to ψ, and $|d| \geq \epsilon_d + \frac{v_f \cdot \tan(\epsilon_\psi)}{K}$, $|d|$ and $|\psi|$ both have finite upper bounds.*

Proof: We borrow the same start time t_0 and initial conditions from Lemma 2. Now that $d(t)$ and $\psi(t)$ are of opposite signs, we can write:

$$V(d(t), \psi(t)) = \begin{cases} |\alpha(d(t))| - |\psi(t)| & |\psi(t)| < |\alpha(d(t))| \\ |\psi(t)| - |\alpha(d(t))| & |\psi(t)| > |\alpha(d(t))| \end{cases}. \tag{16}$$

According to Theorem 2 in Appendix, $|d(t)|$ and $|\alpha(d(t))|$ are both non-increasing, which means $|\alpha(d(t))| \leq |\alpha(d(t_0))| = |\alpha(d_0)|$. In the first case of (16), $|\psi(t)| < |\alpha(d(t))| \leq |\alpha(d_0)|$. By Lemma 1, $V(d(t), \psi(t))$ is monotonically decreasing. Then, in the second case of (16), $|\psi(t)|$ must be non-increasing $\big(|\psi(t)| \leq |\psi(t_0)| = |\psi_0|\big)$. □

Lemma 4. *When (d, ψ) stays in UE, $|d|$ has finite upper bounds.*

Proof: We borrow the same start time t_0 and initial conditions from Lemma 2. We can first divide UE according to the value of $|d|$. $|d|$ is obviously bounded when $|d| < \epsilon_d + \frac{v_f \cdot \tan(\epsilon_\psi)}{K}$. When $|d| \geq \epsilon_d + \frac{v_f \cdot \tan(\epsilon_\psi)}{K}$, we can divide into the following two cases:

- $\frac{dV^2}{dt} < 0$: This case can fall to the proof in Lemma 2 when $d(t)$ and $\psi(t)$ are of the same sign. Otherwise, it can fall to the proof in Lemma 3.
- $\frac{dV^2}{dt} \geq 0$: We can assume an extreme case where $\frac{dV^2}{dt}$ is always positive. That is to say, $|\psi(t) + \alpha(d(t))|$ keeps increasing for $t \geq t_0$. Geometrically, this means the point $(d(t), \psi(t))$ has an increasing distance from the black solid curve in Figure 4. Nevertheless, for each of E_1, E_2, E_3 and E_4, the margin with respect to the black curve is decreasing as $|d|$ increases. As a result, the vehicle state $(d(t), \psi(t))$ will exit UE at some moment $t_1 \geq t_0$. This also implies a finite upper bound for $|d(t)|$ theoretically exists, while the vehicle's state stays in UE.

In this way, we can see a finite upper bound for $|d|$ exists, no matter which part of UE the vehicle state resides in. □

C. Safety Margins of Stanley Controller

For the whole state space inside the nominal region, we can divide it into the following four parts:

- UE
- R_1: the region in Lemma 2
- R_2: the region in Lemma 3
- R_3: the region in SE, where d is of the opposite sign to ψ and $|d| < \epsilon_d + \frac{v_f \cdot \tan(\epsilon_\psi)}{K}$.

R_1, R_2 and R_3 constitute safe ODD. While the car is following the reference path, its states $(d(t), \psi(t))$ can transfer within these four regions and thus spend a certain amount of time inside each of them. The crosstrack error d is obviously bounded while $(d(t), \psi(t))$ is in R_3. Lemma 2 and 3 show that d has explicit upper bounds while $(d(t), \psi(t))$ is in R_1 or R_2. d is also proved to be bounded in UE by Lemma 4. Consequently, at any time moment, a safety margin around the most curved reference path (infinitely large curvature) always exists under the disturbance of perception noise. As a result, $(d(t), \psi(t))$ stays within a certain distance from the equilibrium point.

IV. Impact of Vehicle Parameters

A. Vehicle Speed

By looking at the definitions of E_1, E_2, E_3 and E_4, we can see that the areas of these regions are mainly determined by the terms $arctan\big(L(\frac{sin(\epsilon_\psi)}{d} \pm \frac{Kv_f}{v_f^2+K^2d^2})\big)$ and $arctan\big(L(\frac{1}{d} \pm \frac{Kv_f \cdot sin(\delta_{max})}{v_f^2+K^2d^2})\big)$ respectively, for a specific value of the crosstrack error d. For each of the four regions, the area will be smaller and thus more state space can have safety guarantees from Lemma 1, when $\frac{Kv_f}{v_f^2+K^2d^2}$ is smaller. Given the fact that v_f represents the positive forward speed, we have:

$$\lim_{v_f \to 0^+} \frac{Kv_f}{v_f^2 + K^2d^2} = \lim_{v_f \to +\infty} \frac{Kv_f}{v_f^2 + K^2d^2} = 0, \tag{17}$$

$$\arg\max_{v_f > 0} \frac{Kv_f}{v_f^2 + K^2d^2} = K|d|. \tag{18}$$

The vehicle cannot stay still (zero velocity) or go infinitely fast ($v_f \to \infty$), as indicated by (17). Let's assume the vehicle's minimally allowed speed v_{min} and maximally allowed speed v_{max}. There are then three cases, according to (18):

- $K|d| < v_{min}$: When the vehicle is very close to the reference path, the crosstrack error signal can be easily distorted by perception noise, which makes the safety guarantee in Lemma 1 hard to accomplish (as reflected by Lemma 3). It's better for the vehicle to choose larger speeds and travel across more distances along the reference path.
- $v_{min} \leq K|d| \leq v_{max}$: With respect to safety, the vehicle should go at either v_{min} or v_{max}. If the vehicle needs a shorter path completion time, v_{max} is a better choice.
- $K|d| > v_{max}$: $v_f = v_{min}$ can produce more safety guarantees. If the car still moves at high speeds when

it's far away from the reference path, the path and car will diverge from each other at higher rates.

B. Controller Gain and Vehicle Length

For specific values of v_f and d, we have:

$$\arg\max_{K>0} \frac{Kv_f}{v_f^2 + K^2 d^2} = \frac{v_f}{|d|}.$$

Hence, in terms of creating more safety guarantees, a lower K is better for high speeds and low crosstrack errors, and a higher K is better for low speeds and high crosstrack errors.

The areas of E_1, E_2, E_3 and E_4 become larger when L becomes larger. This is because longer vehicles are harder to safely control, as reflected by the equation $\dot{\theta} = \frac{v_f tan(\delta)}{L}$ [11]. The car's heading direction changes slower for larger L, under the same speed and steering angle.

V. Simulations

We use Matlab and Simulink to carry out simulations and thus validate the safety of the Stanley controller, under the impacts of path curvatures and sensing noise. We first use Matlab scripts to define related parameters, whose values are shown in Table I. Specifically, the reference path is a circle centered at the origin, with a radius of 2.5 (the red curve in Figure 6). The car tries to follow the red circle curve clockwise and thus the path curvature $c(s) = -0.4, \forall s \geq 0$.

Parameters	Values	Descriptions
v_f	2.8	Constant forward velocity (m/s)
L	1.75	Vehicle length (m)
K	0.45	Stanley controller gain
$c(s)$	-0.4	Path curvature (rad/m)
ϵ_d	0.3	Maximum crosstrack noise (m)
ϵ_ψ	$\frac{\pi}{18}$ $(10°)$	Maximum heading noise (rad)
δ_{max}	1.4	Maximum steering angle (rad)

TABLE I

Parameters for the vehicle, reference path and sensing noise.

Then, we use Simulink to build the Stanley controller. This includes two random number generators that produce additive noise to crosstrack and heading error signals respectively, within the assumed ranges $\big([-\epsilon_d, \epsilon_d]$ and $[-\epsilon_\psi, \epsilon_\psi]\big)$. In particular, we carry out two trials, whose vehicle initial states are shown in Table II and visualized in Figure 6.

We run the built model for 9 seconds and the results are shown in Figure 7. In both trials, the car gradually becomes closer to the reference path. Similarly, the heading error ψ converges to a certain level and then stays stable in both trials.

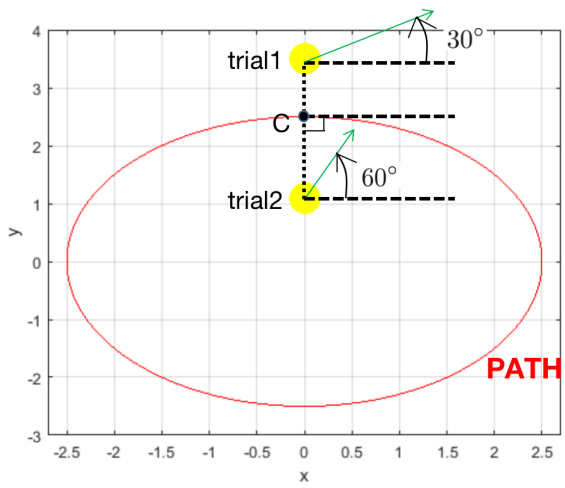

Fig. 6. Reference path and initial states of the vehicle. (The arrows represent the car's heading directions. Point **C** represents the car's initial critical point.)

Trials	1	2
Initial position	$(0, 3.5)$	$(0, 1.1)$
Initial critical point	$(0, 2.5)$	$(0, 2.5)$
Initial crosstrack error (d)	1.0	-1.4
Initial heading error (ψ)	$\frac{\pi}{6}$ $(30°)$	$\frac{\pi}{3}$ $(60°)$

TABLE II

The car's initial states during simulations.

VI. Conclusions

Our work formally adds road curvatures and perception noise into the safety analysis of the popular Stanley controller. By identifying and analyzing extreme cases (of curvature and sensor noise), we're able to show a region (safe ODD), in which the tracking errors are bounded. This formally establishes Stanley's safety in realistic environments. The assumptions and the analysis are conservative (roads cannot have arbitrarily large curvatures and the perception system is unlikely to consistently produce noise of the highest level). Simulation results also validate our theoretical conclusions about Stanley's safety. We also show different speeds are suitable for the vehicle's safety under different vehicle states. Additionally, we derive the relationships among the optimal controller gain, the vehicle speed and the tracking errors. These results can make engineers more informed when choosing design parameters.

Furthermore, our work has revealed several interesting future work directions. On the Lyapunov analysis side, we can design new Lyapunov functions and even combine different Lyapunov functions together for a more accurate analysis. On the noise model side, we can work with hardware and sensor engineers to bring more practical noise models into our analysis, as the sensing noise can be state-dependent [6]. On the controller design side, we can use the insights from our

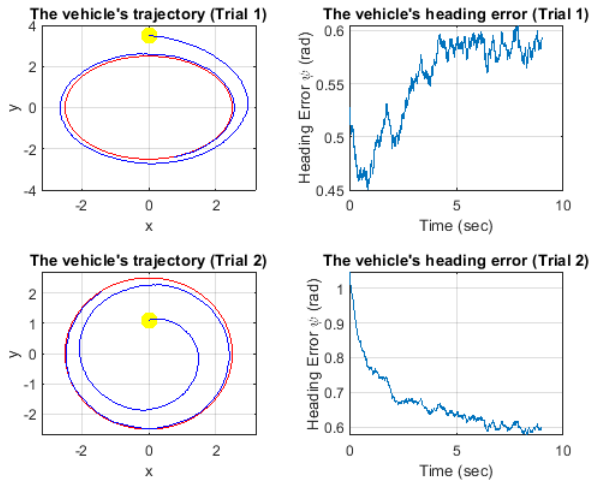

Fig. 7. Running results of the simulations.

analysis to create longitudinal dynamics and hereby replace the constant forward speed in the original Stanley model. We can also add in other constraints like maximally allowed crosstrack errors and speed limits to set up an optimal control problem for the minimum completion time.

REFERENCES

[1] G. M. Hoffmann, C. J. Tomlin, M. Montemerlo, and S. Thrun. Autonomous Automobile Trajectory Tracking for Off-Road Driving: Controller Design, Experimental Validation and Racing, *2007 American Control Conference*, New York, NY, USA, 2007, pp. 2296-2301, doi: 10.1109/ACC.2007.4282788.

[2] S. Thrun *et al.* (2007). Stanley: The Robot That Won the DARPA Grand Challenge. In: M. Buehler, K. Iagnemma, and S. Singh (eds) *The 2005 DARPA Grand Challenge*. Springer Tracts in Advanced Robotics, vol 36. Springer, Berlin, Heidelberg. https://doi.org/10.1007/978-3-540-73429-1_1.

[3] N. Amer, H. Zamzuri, K. Hudha, V. Aparow, Z. Kadir, and F. A. Zainal, (2018). Path tracking controller of an autonomous armoured vehicle using modified Stanley controller optimized with particle swarm optimization. *Journal of the Brazilian Society of Mechanical Sciences and Engineering*. 40. 10.1007/s40430-017-0945-z.

[4] L. Wang, Z. Zhai, Z. Zhu, and E. Mao. Path Tracking Control of an Autonomous Tractor Using Improved Stanley Controller Optimized with Multiple-Population Genetic Algorithm. *Actuators*. 2022; 11(1):22. https://doi.org/10.3390/act11010022.

[5] A. AbdElmoniem, A. Osama, M. Abdelaziz, and SA. Maged. A path-tracking algorithm using predictive Stanley lateral controller. *International Journal of Advanced Robotic Systems*. 2020;17(6). doi:10.1177/1729881420974852.

[6] C. Hsieh, Y. Li, D. Sun, K. Joshi, S. Misailovic, and S. Mitra, Verifying Controllers With Vision-Based Perception Using Safe Approximate Abstractions, in *IEEE Transactions on Computer-Aided Design of Integrated Circuits and Systems*, vol. 41, no. 11, pp. 4205-4216, Nov. 2022, doi: 10.1109/TCAD.2022.3197508.

[7] S. L. Herbert, M. Chen, S. Han, S. Bansal, J. F. Fisac, and C. J. Tomlin, FaSTrack: A modular framework for fast and guaranteed safe motion planning, *2017 IEEE 56th Annual Conference on Decision and Control (CDC)*, Melbourne, VIC, Australia, 2017, pp. 1517-1522, doi: 10.1109/CDC.2017.8263867.

[8] S. Kousik, S. Vaskov, F. Bu, M. Johnson-Roberson, and R. Vasudevan. Bridging the gap between safety and real-time performance in receding-horizon trajectory design for mobile robots. *The International Journal of Robotics Research*. 2020;39(12):1419-1469. doi:10.1177/0278364920943266.

[9] T. D. Gillespie. *Fundamentals of Vehicle Dynamics*, Society of Automotive Engineers, Warrendale, PA, 1992.

[10] A. D. Luca, G. Oriolo, and C. Samson, (1998). Feedback control of a nonholonomic car-like robot. In: Laumond, J.P. (eds) *Robot Motion Planning and Control*. Lecture Notes in Control and Information Sciences, vol 229. Springer, Berlin, Heidelberg. https://doi.org/10.1007/BFb0036073.

[11] J. M. Snider, (2009). *Automatic Steering Methods for Autonomous Automobile Path Tracking*. Research Report CMU-RI-TR-09-08, Carnegie Mellon University, 2009.

[12] B. Paden, M. Cap, S. Z. Yong, D. Yershov, and E. Frazzoli. A Survey of Motion Planning and Control Techniques for Self-Driving Urban Vehicles, in *IEEE Transactions on Intelligent Vehicles*, vol. 1, no. 1, pp. 33-55, March 2016, doi: 10.1109/TIV.2016.2578706.

[13] M. Abraham, A. Mayne, T. Perez, I. R. De Oliveira, H. Yu, C. Hsieh, Y. Li, D. Sun, and S. Mitra. Industry-track: Challenges in Rebooting Autonomy with Deep Learned Perception, *2022 International Conference on Embedded Software (EMSOFT)*, Shanghai, China, 2022, pp. 17-20, doi: 10.1109/EMSOFT55006.2022.00016.

APPENDIX

Theorem 1. *When* $d > 0$, $\frac{cos(e_\psi+\alpha(d_s))c(s)}{1-d\cdot c(s)} < \frac{sin(\epsilon_\psi)}{d}$. *When* $d < 0$, $\frac{cos(e_\psi+\alpha(d_s))c(s)}{1-d\cdot c(s)} > \frac{sin(\epsilon_\psi)}{d}$.

Proof: To create the worst cases where the reference path is always curving away from the vehicle, we let $c(s) \leq 0$ for $d > 0$ and vice versa, as illustrated in Figure 8. When $d \in$

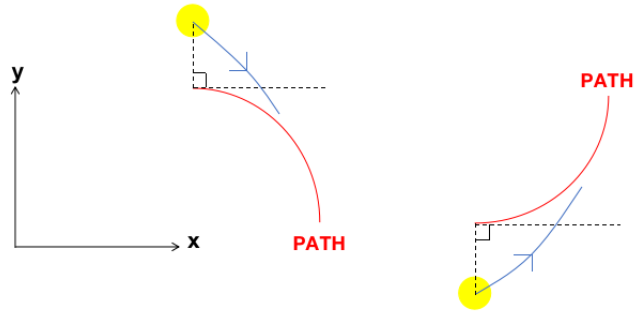

Fig. 8. Left: $d > 0$, $c(s) < 0$. Right: $d < 0$, $c(s) > 0$.

$(0, +\infty)$, $d_s \in (-\epsilon_d, +\infty)$. Hence, $\alpha(d_s) \in (-\alpha(\epsilon_d), \frac{\pi}{2})$ and thus $e_\psi + \alpha(d_s) \in (-\epsilon_\psi - \alpha(\epsilon_d), \frac{\pi}{2} + \epsilon_\psi)$. Considering Assumption 1, we can get $-\frac{\pi}{2} < -\delta_{max} < -\epsilon_\psi - \alpha(\epsilon_d) < e_\psi + \alpha(d_s) < \frac{\pi}{2} + \epsilon_\psi < \pi$. From the trigonometry, we can get $cos(e_\psi + \alpha(d_s)) > cos(\frac{\pi}{2} + \epsilon_\psi) = -sin(\epsilon_\psi)$ and thus $\frac{cos(e_\psi+\alpha(d_s))c(s)}{1-d\cdot c(s)} < \frac{sin(\epsilon_\psi)c(s)}{d\cdot c(s)-1}$.

Over the domain $c(s) \in (-\infty, 0]$, $\frac{sin(\epsilon_\psi)c(s)}{d\cdot c(s)-1}$ is monotonically decreasing. Hence,

$$\frac{cos(e_\psi + \alpha(d_s))c(s)}{1 - d\cdot c(s)} < \frac{sin(\epsilon_\psi)c(s)}{d\cdot c(s) - 1} < \lim_{c(s)\to-\infty} \frac{sin(\epsilon_\psi)c(s)}{d\cdot c(s) - 1} = \frac{sin(\epsilon_\psi)}{d}.$$

The proof is similar when $d < 0$. □

Theorem 2. *When* $|d| \geq \epsilon_d + \frac{v_f\cdot\tan(\epsilon_\psi)}{K}$, $|d|$ *and* $|\alpha(d)|$ *are both non-increasing.*

Proof: For positive values, $d \geq \epsilon_d + \frac{v_f\cdot\tan(\epsilon_\psi)}{K}$, which implies $-\epsilon_\psi + \alpha(d - \epsilon_d) \geq 0$. By combining this with (2), we get:

$$e_\psi + \alpha(d_s) \geq -\epsilon_\psi + \alpha(d - \epsilon_d) \geq 0. \tag{19}$$

By plugging (19) into (4) and (5), we can conclude $\dot{d} \leq 0$ and $\dot{\alpha}(d) \leq 0$. The proof for negative values of d is similar. □